Volume 16
Number 44
28 November 2025
Pages 4777-4854

Polymer Chemistry

rsc.li/polymers

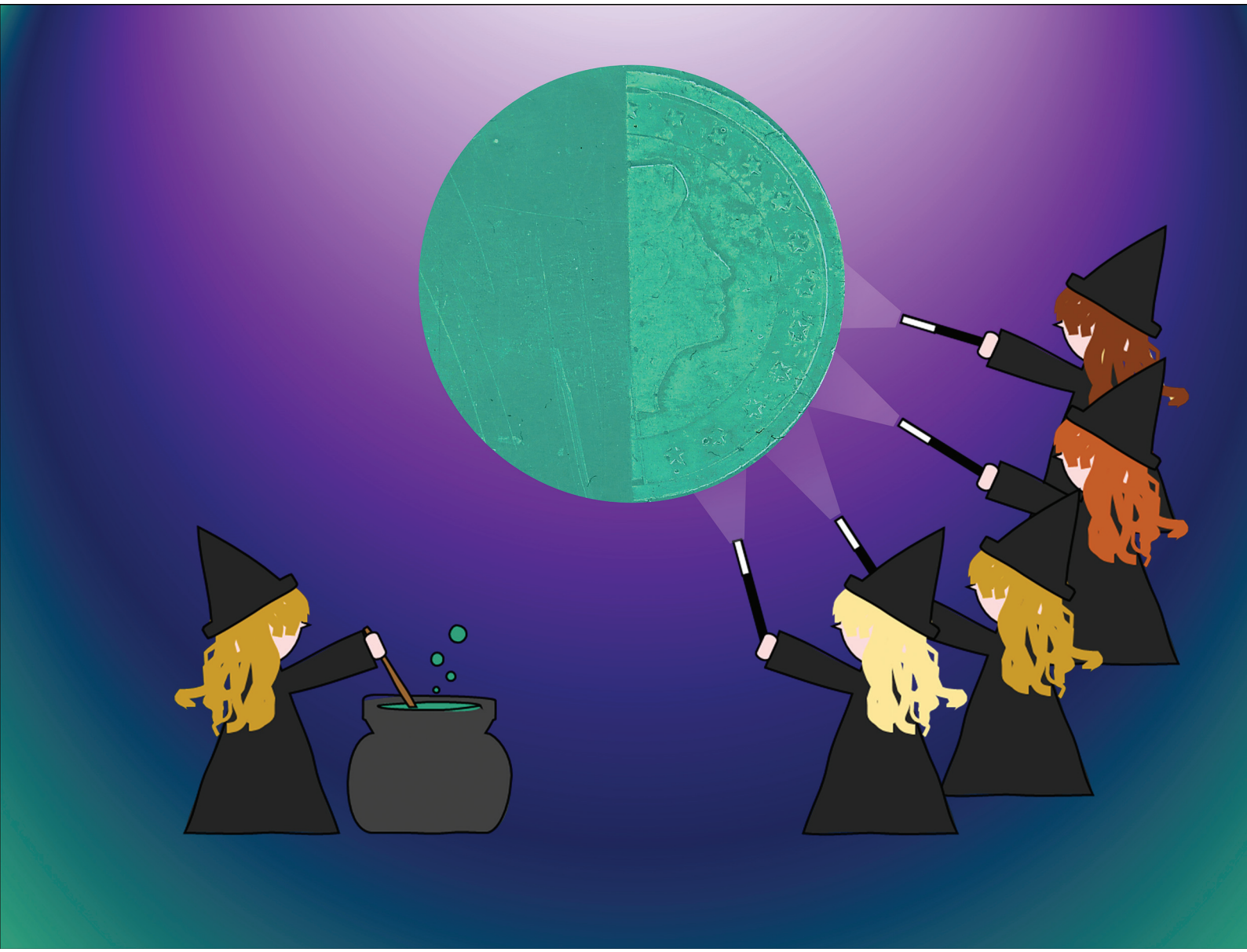

ISSN 1759-9962

ROYAL SOCIETY OF CHEMISTRY

PAPER
Elisabeth Rossegger *et al.*
Synthesis of tetramethylguanidine-based photobase generators: light-guided dynamics in thioester networks

15 YEARS ANNIVERSARY

Polymer Chemistry

PAPER

View Article Online
View Journal | View Issue

Cite this: *Polym. Chem.*, 2025, **16**, 4783

Synthesis of tetramethylguanidine-based photobase generators: light-guided dynamics in thioester networks

Pia-Maria Egger, [a,b] Hannah Sivetz,[b] Simon Renner,[a,b] Roman Korotkov,[a] Christoph Schmidleitner, [a,b] Marco Sigl, [b] Inge Mühlbacher,[a,b] Gregor Trimmel, [b] Sandra Schlögl [a] and Elisabeth Rossegger *[a,b]

Covalent adaptable networks are crosslinked structures with bonds that undergo reversible exchange reactions when exposed to an external stimulus, enabling a reorganization of their topology. The incorporation of photolatent catalysts allows precise tuning of viscoelastic properties and on-demand activation. Herein, the local control of dynamic bond exchange reactions in thiol–ene resins, bearing thioester linkages and free thiol groups, was investigated, by synthetizing numerous tetramethylguanidine (TMG) based photobase generators with varying UV-Vis absorption profiles to improve the orthogonality between curing reaction and photobase activation. UV-induced activation of the photolatent base yields a strong guanidine base, which is able to efficiently catalyze thiol–thioester exchange reactions. Rheological studies, combined with pH measurements upon UV activation of the bases, identified the most promising photolatent base 1,1,3,3-tetramethylguanidine 2-(naphthalen-2-yl)-2-oxoacetate (**TMG-NOA**). In addition to light, also temperature can be used to activate **TMG-NOA** that further increases its applicability. The influence of the developed photobases on the material properties and the curing kinetics were investigated using FTIR- spectroscopy, TGA and DSC measurements. Utilizing the network containing **TMG-NOA**, the spatially controlled activation of the thiol–thioester exchange mechanism in selected areas was demonstrated at temperatures between 40–70 °C through local imprinting experiments, photochemical drawing and thermally induced healing.

Received 5th August 2025,
Accepted 30th September 2025

DOI: 10.1039/d5py00779h

rsc.li/polymers

Introduction

Traditional thermosets are permanent, rigid, and chemically crosslinked polymers making them well-suited for structural and high-temperature applications but due to their irreversible nature, recycling and reprocessing of these polymers is rather difficult. Covalent adaptable networks (CANs) overcome these limitations by combining the properties of thermosets with the dynamics of controllably reversible bonds.[1] The general production of CANs is carried out by incorporating labile chemical bonds into the network. These bonds are subsequently triggered by an external stimulus (light or heat), and can follow two pathways. They can either break and reform following a reversible addition or dissociative mechanism, or they can interconvert following a reversible exchange or an associative mechanism.[2–5] In particular, CANs containing thiol–ene click chemistry exhibit excellent properties such as insensitivity to oxygen,[6] compatibility with various functional groups, quantitative conversions[7] and environmental friendliness.[8–10] The literature reports various types of dynamic exchange mechanisms for thiol–ene networks, including thiol–thioester exchange,[11,12] transesterification[13,14] and disulfide exchange.[14,15] Notably, thiol–thioester exchange reactions demonstrate efficient and often stoichiometric exchanges of functionalities at low concentrations, occurring rapidly under mild reaction conditions.[4] These dynamic networks are utilized in photolithography,[10,16] microdevice fabrication,[17,18] optical[17] and electronic devices[19] as well as biomedical applications.[20,21] In 2018 Bowman *et al.* reported the light-mediated activation of thioester-based networks using a UV-deprotectable base, resulting in an on-demand spatial and temporal control of the thiol–thioester exchange mechanism in the network. In the following years, our research group also investigated this topic and contributed additional findings. We were able to adapt and implement the concept, of the spatial on-demand activation of base-catalyzed exchange mechanism, within the framework of the transesterification mechanism,

[a]*Polymer Competence Center Leoben GmbH (PCCL), Sauraugasse 1, 8700 Leoben, Austria. E-mail: elisabeth.rossegger@pccl.at*
[b]*Graz University of Technology, Institute of Chemistry and Technology of Materials, Stremayrgasse 9, 8010 Graz, Austria*

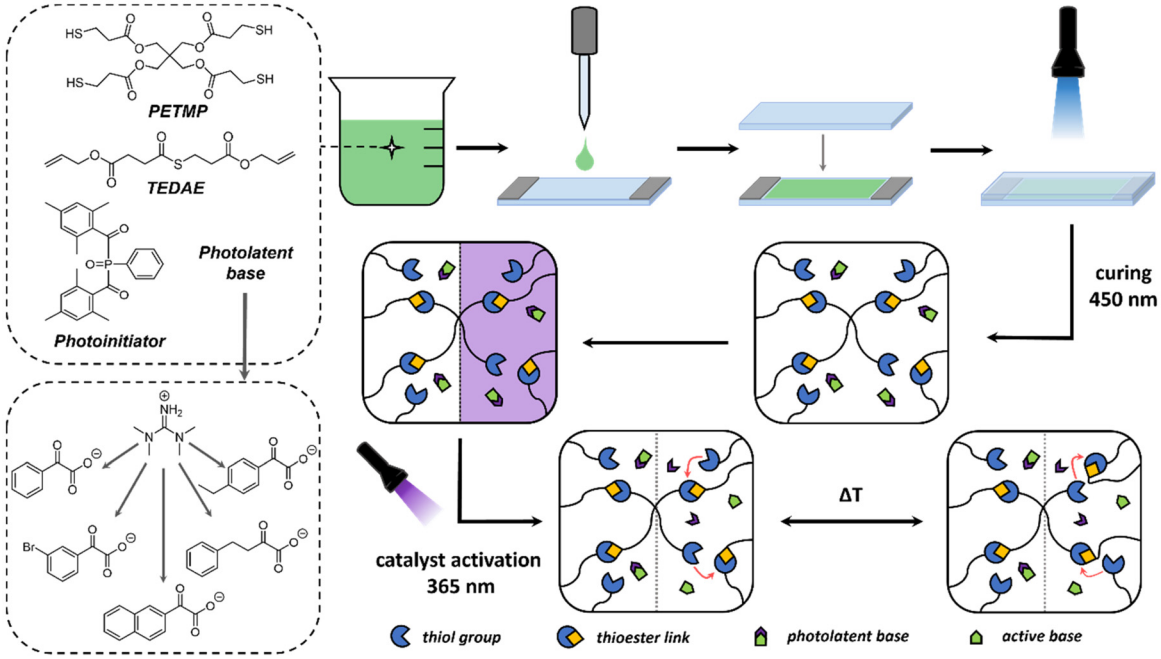

Fig. 1 General scheme for the manufacturing process of the dynamic thiol–ene network: curing of the formulation between two glass slides using 450 nm UV-light followed by a spatial activation (365 nm UV-light) of the photolatent base and thermally activated thiol–thioester exchange.

which is based on the dynamic bond exchange of ester links and hydroxy groups.[13,22,23] Recent findings from our group have also confirmed that spatial and reversible control of the thiol–thioester mechanism in a thiol–ene network can be achieved by utilizing a photoswitchable nitrogen superbase.[24] Since thiol–thioester networks are especially convenient for biomedical applications due to their rapid reaction at low temperatures in the presence of suitable catalysts, we direct our investigation towards these systems.[11] Within subsequent studies, the focus will be placed on the spatially resolved on-demand activation of thiol–thioester exchange reactions using photolatent bases (PLBs). The general principle includes the light-mediated cleavage of a PLB, which leads to the release of a strong base. Through that, one can spatiotemporally control the onset of dynamic bond exchange.[5,22] Herein, we synthesized thioester-bearing vinyl monomers to enable network formation upon exposure to 450 nm UV-light *via* a thiol–ene-click reaction. The primary aim was to develop a photobase that, once incorporated into the network, enables improved spatial control over the thiol–thioester exchange reaction through its UV-Vis properties and pH changes. To achieve this spatial resolution, a library of TMG-based photobase generators (TMG-PLBs) were synthesized. These TMG-PLBs incorporate 1,1,3,3-tetramethylguanidine as a strong base, along with phenylglyoxylic acid or its derivatives, which are modified with spacers or side groups. The activation of the photolatent bases in the network was carried out by irradiation with 365 nm UV-light. To enable spatial control over the dynamic exchange reaction, it is essential that the curing of the polymer network and the activation of the photolatent base occur independently. The general concept of these networks is illustrated in Fig. 1 providing a detailed overview of the synthesized bases, the network components as well as the overall workflow. Further insight into the properties and trends of the photolatent bases was gained by UV-Vis measurements in acetonitrile and continuous pH measurements in methanol under 365 nm UV-light irradiation. Additionally, a detailed examination of the networks through stress relaxation studies revealed the most suitable photolatent base for this application. The dynamic behavior of the network containing 1,1,3,3-tetramethylguanidine 2-(naphthalen-2-yl)-2-oxoacetate (**TMG-NOA**) was the most promising, showing fast reaction rates even at 40 °C after UV-light activation and nearly no relaxation without activation. Additionally, imprinting, photochemical drawing and healing experiments were carried out to macroscopically demonstrate the spatially resolved dynamic properties of this system.

Results and discussion

Synthesis and characterization of photolatent bases

The photolatent bases containing 1,1,3,3-tetramethylguanidine[4] as a strong base, along with phenylglyoxylic acid or its derivatives were synthesized in an modified manner according to the literature.[22] ^{1}H and ^{13}C NMR spectra (Fig. S1–S6, SI) correspond to the proposed structures presented in Fig. 1. UV-Vis measurements of the photolatent bases were performed to demonstrate their photochemical reactivity, revealing that the PLBs are inactive at 450 nm. This is particularly significant, to enable a local control and on-demand activation of dynamic thio–thioester exchange reactions as network formation is

triggered by the photoinitiator (phenylphosphoryl)bis(mesitylmethanone) (**BAPO**) upon 450 nm light irradiation. UV-Vis adsorption spectra were measured at concentrations of 1×10^{-3} mol L^{-1} (Fig. 2a) and 1×10^{-4} mol L^{-1} (Fig. 2b) of TMG-PLB in acetonitrile. The UV-Vis spectra with concentrations of 1×10^{-3} mol L^{-1}, show similar absorptions for 1,1,3,3-tetramethylguanidine phenylglyoxylate (**TMG-PGO**, λ_{max} = 377 nm), 1,1,3,3-tetramethylguanidine 2-(4-bromophenyl)-2-oxoacetate (**TMG-BOA**, λ_{max} = 381 nm) and 1,1,3,3-tetramethylguanidine 2-(4-ethylphenyl)-2-oxoacetate (**TMG-EOA**, λ_{max} = 371 nm) in acetonitrile. 1,1,3,3-tetramethylguanidine 4-phenylbutoxy acetate (**TMG-PBA**, λ_{max} = 321 nm) exhibits the lowest absorption at 365 nm due to the presence of an additional $-CH_2$ group, which spatially and electronically decouples the phenyl ring from the carbonyl moiety, thereby interrupting the direct π-conjugation. 1,1,3,3-Tetramethylguanidine 2-(naphthalen-2-yl)-2-oxoacetate (**TMG-NOA**, λ_{max} = 325 nm, 338 nm, 378 nm), on the other hand, shows the highest absorption at 365 nm and the largest red shift, attributed to its higher number of conjugated carbon double bonds, which results in enhanced π-conjugation. The UV-Vis spectra with concentrations of 1×10^{-4} mol L^{-1}, exhibit a significantly higher absorption at 250 nm for the **TMG-BOA** (λ_{max} = 251 nm), due to electron-withdrawing effect of the attached bromine, compared to **TMG-EOA** (λ_{max} = 250 nm). At this concentration, **TMG-PGO** (λ_{max} = 218 nm) and **TMG-PBA** (λ_{max} = n/a) display relatively low absorptions compared to the other TMG-PLBs. **TMG-NOA** (λ_{max} = 283 nm, 324 nm, 338 nm) again demonstrates the highest red shift in absorption at the concentration of 1×10^{-4} mol L^{-1}.

Additionally, pH measurements in methanol were carried out to investigate the activation behavior of the TMG-PLBs (Fig. 2c). All solutions were initially irradiated at 450 nm to demonstrate the photolatent bases' inactivity at this wavelength, as summarized in Table S1 in SI. Generally, all of the TMG-PLBs show already basic initial pH values, this may be attributed to the equilibrium between the carboxylate salt and the free acid/amine. The activation mechanism under 365 nm UV irradiation involves an initial homolytic cleavage of the C–C bond, generating a benzoyl radical and a $(CO_2HNR_3)^{\bullet}$ species (Fig. 2d). Subsequent hydrogen transfer to the benzoyl radical yields an aldehyde, while the guanidine base is simultaneously released and carbon dioxide is generated.[25] The principle is applicable to all the photobases synthetized herein, with the exception of TMG-PBA. The introduction of additional $-CH_2$ groups between the phenyl ring and the carbonyl moiety interrupts the direct π-conjugation between these functional groups. Consequently, the C–C bond cleavage

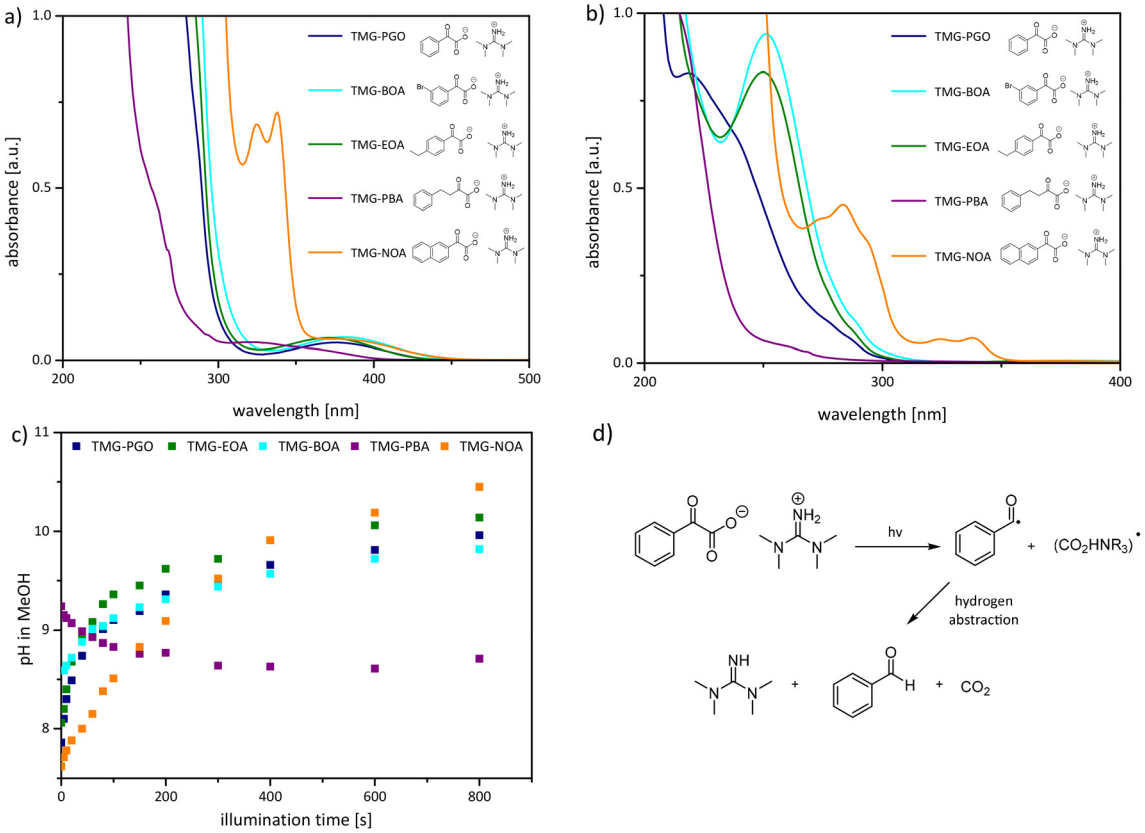

Fig. 2 (a) UV-Vis absorption spectra of TMG-PLBs 1×10^{-3} mol L^{-1} in acetonitrile. (b) UV-Vis absorption spectra of TMG-PLBs 1×10^{-4} mol L^{-1} in acetonitrile. (c) pH measurements of TMG-PLBs in methanol (0.06 mol L^{-1}) upon irradiation with 365 nm UV-light. (d) Activation mechanism of the TMG-PLB with **TMG-PGO** as example.[25]

becomes energetically less favorable. As reported in literature, the presence of α-hydrogen can lead to an enol-acid tautomerization.[26] The pH measurements clearly indicate that **TMG-NOA** is the most advantageous, as it initially exhibits a pH of 7.6 and subsequently transitions to a highly basic condition (pH 10.5) upon irradiation. A summary of the pH values over the irradiation time of 800 s can be found in Table S1 in SI. A general trend in efficiency can be defined as follows:

TMG-NOA > **TMG-EOA** > **TMG-PBA** ~ **TMG-BOA** >> **TMG-PBA**.

Thermogravimetric analysis was carried out to determine the thermal stability of the photolatent bases (Fig. S7, SI). **TMG-PGO**, **TMG-BOA** and **TMG-EOA** exhibit similar behavior with a total mass loss of 5% within the temperature range of 160–174 °C. In contrast, **TMG-PBA** and **TMG-NOA** exhibit a lower thermal stability. **TMG-NOA** displays a total mass loss of 15% at 162 °C, which corresponds to the release of CO_2 and leads to the idea that also temperature can be used to activate the photobase. To further investigate the thermal activation behavior of **TMG-NOA** in the network we measured the stress relaxation at 70 °C of a thermally activated sample (125 °C for 30 minutes), resulting in a slow relaxation to $1/e$ in 8000 s (Fig. S8, SI). Therefore, thermal activation is generally possible for **TMG-NOA** under suitable conditions, that further enhances the applicability of the synthesized base as also temperature can be used as an external stimulus for activation.

Curing kinetics

The pentaerythritol-tetrakis(3-mercaptopropionate) (**PETMP**), containing four thiol groups and a thioester (**TEDAE**), containing two diene functionalities were used in an equimolar amount (1 : 1). This ratio was chosen to promote network formation *via* thiol–ene click reaction under visible light, while the excess thiol groups from PETMP allow for subsequent thiol–thioester exchange within the network. To enable light-induced thiol–ene click polymerization, BAPO was added as photoinitiator in a concentration of 1 mol% relative to the thiol functions. The photolatent bases (TMG-PLBs) were incorporated in a concentration of 3 mol% relative to the thiol groups. To gain detailed insights into the reaction kinetics and carbon double bond conversion, FT-IR spectroscopy measurements were performed. A clear decrease in the alkene absorption bands at 1630–1660 cm^{-1} was observed throughout the curing process. The resulting double bond conversion (Fig. 3) was calculated from the integrals of the stretching vibration of the C=C bonds at 1630–1660 cm^{-1} normalized by the carbonyl peak C=O at 1710–1780 cm^{-1}. By comparing the resins with the varying photolatent bases, it can be observed that they reach similar maximum conversions at irradiation of 1800 s. The maximum conversions reached are summarized in Table S2 in SI. Additionally, the FTIR spectra for the thiol–ene network containing **TMG-NOA** is provided in the SI (Fig. S9, SI). The final thiol conversion was not determined, since an excess of –SH groups was used in the resin to provide free thiols for the thiol–thioester exchange reaction.

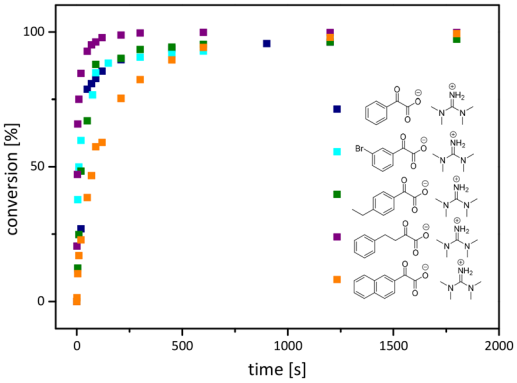

Fig. 3 Carbon double bond conversion [%] plotted against the irradiation time [s] with 450 nm UV-light.

In general, these types of photolatent bases function as an internal filter, meaning that they absorb photons, leading to a slower curing process without being photoactivated themselves at 450 nm UV-light, proven by pH measurements upon 450 nm irradiation. An analysis of the conversion rates (Fig. 3) shows a similar trend to that observed in the UV-Vis spectra (Fig. 2a and b). **TMG-PBA** shows the highest curing rate which corresponds well to the low absorbance, whereas **TMG-NOA** exhibits the slowest curing rate and the highest absorbance. **TMG-PGO**, **TMG-BOA** and **TMG-EOA** display similar curing rates which coincide with the trends seen in the absorption spectra (Fig. 2a and b). Overall, all of the mentioned networks show fast curing rates, leading to nearly full double bond conversion within 600 s.

Thermomechanical network properties

Thermogravimetric analysis was performed to determine the maximum operating temperature of the thiol–ene photopolymer. All networks measured with incorporated TMG-PLBs exhibited similar behavior, with a 5% weight loss occurring at temperatures ranging from 203–252 °C. This mass loss can be attributed to the theoretical mass fraction of the TMG-PLBs in the polymer system. The thiol–ene system itself started to degrade at approximately 300 °C, as confirmed by analyzing a reference sample without the incorporated photolatent base (Fig. 4a). Overall, the networks exhibited thermal stability well beyond the temperature range needed for effective thiol–thioester exchange. Notably, it was observed that the network with **TMG-NOA** shows the highest thermal stability even though the **TMG-NOA** itself showed the lowest thermal stability amongst all the photolatent bases. One possible explanation is that integrating the base into the network allows the thermally generated cleavage products to stay dissolved in the polymer matrix, delaying their evaporation until the temperature exceeds 200 °C. Reisinger *et al.* already observed this effect and employed it strategically to thermally deactivate the stress relaxation of a dynamic network.[22]

Differential scanning calorimetry measurements were carried out to determine the glass transition temperature (T_g)

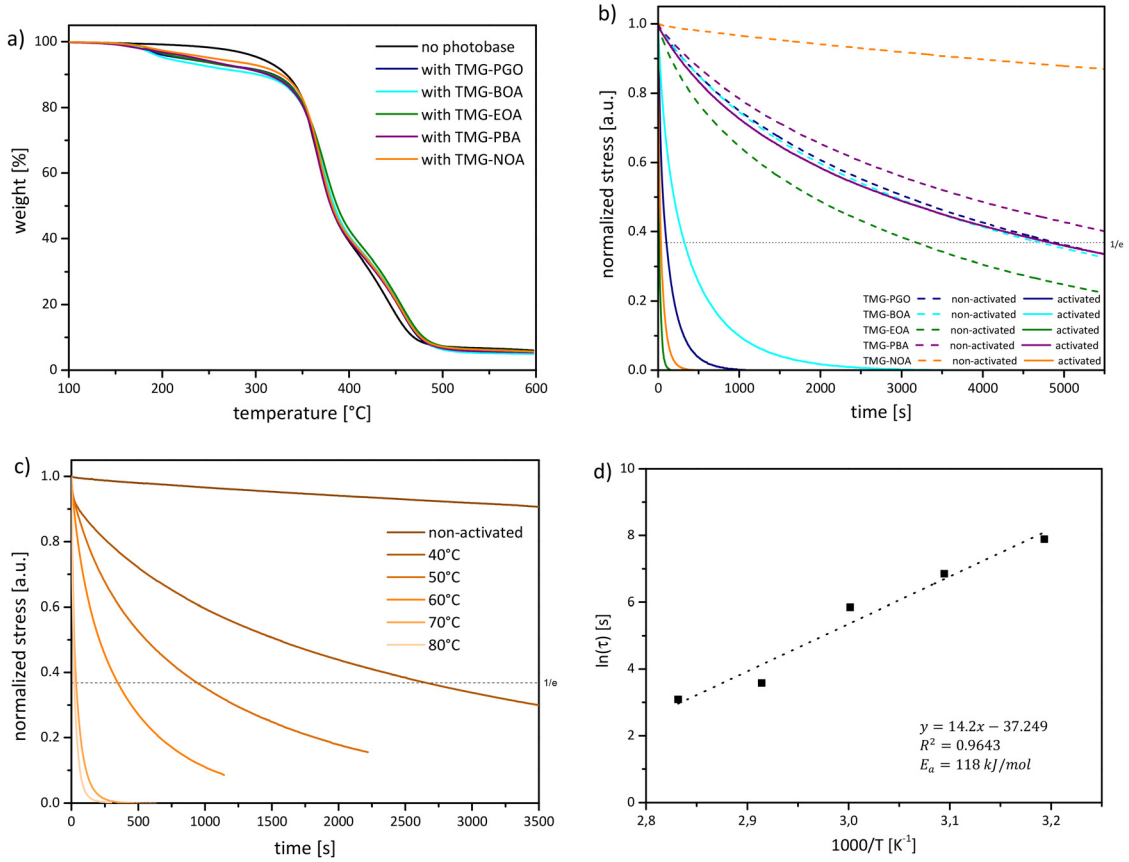

Fig. 4 (a) Thermogravimetric analysis of the cured photopolymer with incorporated TMG-PLBs. (b) Normalized stress relaxation curves of the activated and non-activated networks containing the TMG-PLBs at 70 °C. (c) Normalized stress relaxation curves of the activated network containing **TMG-NOA** at a temperature range of 40 °C–80 °C. (d) Arrhenius plot of the network containing **TMG-NOA**.

of the cured networks with incorporated TMG-PLBs. The networks exhibit similar glass transition temperatures ranging from −35 to −37 °C (Fig. S10–S14, SI) independent from the incorporated base. Furthermore, it was confirmed that the activation process of the photolatent base has only a negligible effect on the resulting network properties. To get better insight in the dynamic properties of the networks, stress relaxation measurements were conducted on covalently crosslinked 0.5 mm thick polymer samples in the linear viscoelastic range of the material with a 3% step strain. The measurements were conducted to demonstrate the efficiency of the thiol–thioester exchange mechanism in the network and to determine if the network curing and base activation proceed independently of one another. Therefore, stress relaxation measurements were performed at 70 °C prior to and after activation of the samples with 365 nm UV-light (Fig. 4b). In the non-activated samples with **TMG-PGO** (relaxation to 1/*e* in 4900 s, pH_{start} = 7.86), **TMG-BOA** (relaxation to 1/*e* in 4710 s, pH_{start} = 8.59), **TMG-EOA** (relaxation to 1/*e* in 3190 s, pH_{start} = 8.06) as well as **TMG-PBA** (relaxation to 1/*e* in 6228 s, pH_{start} = 9.24), stress relaxation can unfortunately be observed, which is a result of their basic starting pH values and partial activation of the base upon curing. As discussed, TMG-PLBs exhibit an equilibrium between the carboxylate salt and the free base/acid, resulting in basic initial pH values and influencing stress relaxation in the non-activated networks. This stress relaxation behavior of the non-activated samples is unfavorable, since it limits the controlled activation of the base. In contrast to the previously mentioned non-activated samples, the sample containing non-activated **TMG-NOA** exhibits negligible stress relaxation, which can be explained through the less basic pH value (pH_{start} = 7.62). The activation of the photolatent base is triggered by 365 nm UV-light irradiation for 1 min per side. The activated network with incorporated **TMG-EOA** (relaxation to 1/*e* in 16 s) exhibits the fastest stress relaxation, however, the non-activated sample already shows significant relaxation due to its initial basic pH of 8.06. Upon activation the pH increases further to 10.14, which accelerates the resulting stress relaxation of the network. The activated network with **TMG-PBA** exhibits the slowest stress relaxation (relaxation to 1/*e* in 4838 s) comparable to the non-activated **TMG-PBA** network, which is attributed to the different photocleavage mechanism, as evidenced by the change of the pH from 9.24 to 8.71 (Fig. 2c). The activated **TMG-PGO** network shows a faster relaxation (relaxation to 1/*e* in 104 s, pH_{final} = 9.96) than **TMG-BOA** (relaxation to 1/*e* in 326 s, pH_{final} = 9.82), which can be explained by the more basic

final pH value observed after activation. As the last aspect to be addressed, the activated network containing **TMG-NOA** exhibits fast stress relaxation in the activated state, which corresponds well to the pH measurement under irradiation (pH_{final} = 10.45), while do not showing a significant stress-relaxation in the non-activated state.

Due to its outstanding relaxation behavior in the activated state and negligible stress relaxation response in the non-activated state, the network with **TMG-NOA** was investigated further at varying temperatures from 40 °C to 80 °C (Fig. 4c). Generally, the stress-relaxation process is accelerated toward higher temperatures since the thiol–thioester exchange proceeds more rapidly. However, in the case of **TMG-NOA**, it can be observed that the network relaxes very well even at lower temperatures, which is especially advantageous for biomedical applications. The resulting values for τ can be obtained at the point $(G_{(t)}/G_{(0)})$ equals $(1/e)$ as a generic exponential decrease. By plotting $\ln(\tau)$ against $(1/T)$, a linear trend according to the Arrhenius relationship is observable, which represents one of the key characteristics of a dynamic polymer network following an associative exchange mechanism (Fig. 4d).

Additionally, the activation energy (E_a) was calculated by multiplying the slope of the linear fit equation with the ideal gas constant R. The resulting E_a of 118 kJ mol^{-1} correlates well with the literature known values for thiol–thioester networks varying from 36–139 kJ mol^{-1} depending on the thiol and network type.[11]

Imprinting, photochemical drawing and healing

To illustrate the spatiotemporal activation of the dynamic exchange mechanism on a macroscopic scale, experiments involving imprinting, photochemical drawing, and healing were conducted with the network containing **TMG-NOA**.

For the imprinting process, films were cured in a silicon mold and then selectively activated on one side with 365 nm UV-light. The films were placed in a Teflon press with 1-euro coins as imprinting objects. The imprinting was then achieved by applying pressure with the Teflon press at 70 °C for 15 minutes. During the imprinting period, the network topology of the activated side was reorganized according to the defined imprint of the coin *via* the base-catalyzed thiol–thioester exchange mechanism. In contrast, the non-activated side did not maintain the imprint due to its physical relaxation above T_g, resulting in the recovery of its original shape. Therefore, a distinct imprint was observed on the activated side, whereas no imprint was visible on the non-activated side, after cooling and pressure release of the Teflon press (Fig. 5).

In the photochemical drawing experiment, a film with bromothymol blue (BTB) as pH indicator was cured with 450 nm UV-light. The incorporated photolatent base **TMG-NOA** was then selectively activated using 365 nm UV-light and a lined (length 6.5 mm, width 0.6 mm) or dotted (diameter 1 mm) photomask to show the maximum resolution achievable. The activated areas (lines or dotted) exhibit a color change from yellow to colorless, indicating the release of the photolatent base and further suggesting pH increase of the dynamic network (Fig. 6). However, it is reported in literature that an increase in pH (pK_a > 7.5) leads to a structural change in BTB, which should result in a blue color. In general, bromothymol blue exhibits a yellow color in weak acidic solutions and it changes to blue *via* green when reaching a higher pH. Additionally, literature reports a structure of bromothymol blue in the acidic region that is colorless, which corresponds well with the visual color change of the film.[27] Therefore, it is hypothesized that the pH of the whole network in the activated state is higher than in the non-activated one, but still remains in the acidic range. The yellow and colorless molecule structures of bromothymol blue are included in the SI (Fig. S16). To prove this concept, zeta-potential measurements were carried out and the obtained data indicates an isoelectric point of 0.83 for the non-activated network and 2.14 for the activated network, which is higher but still in the acidic region (Fig. S15, SI).

To demonstrate the local activation of dynamic exchange reaction on a smaller scale, photopatterned healing experiments were carried out by curing a film with 450 nm UV-light before inserting a small cut (length 15 mm, width 0.1 mm).

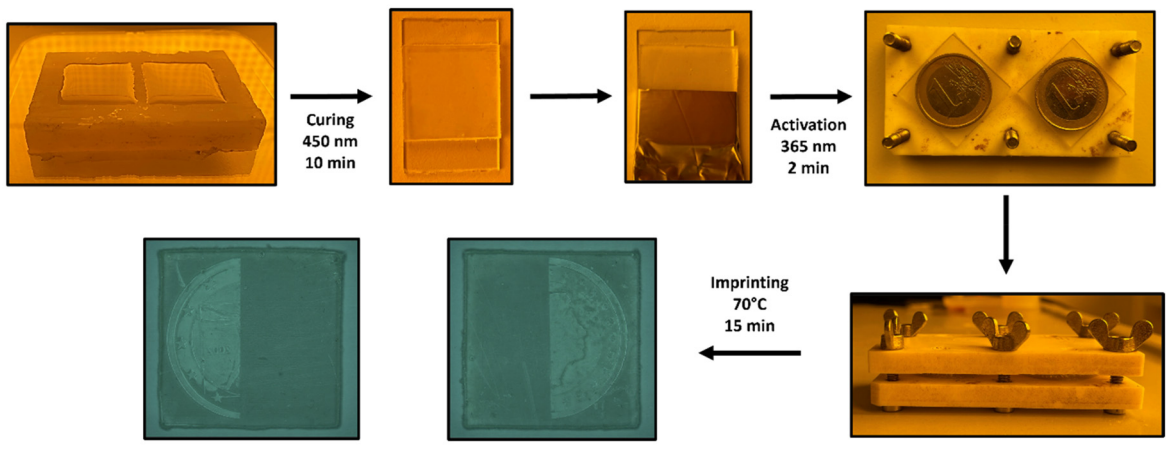

Fig. 5 Imprinting experiment with cured films at 450 nm. One sided spatial activation of the photolatent base **TMG-NOA** was induced with 365 nm UV-light and imprinting of the 1-euro coins was performed by using a Teflon press at 70 °C for 15 minutes.

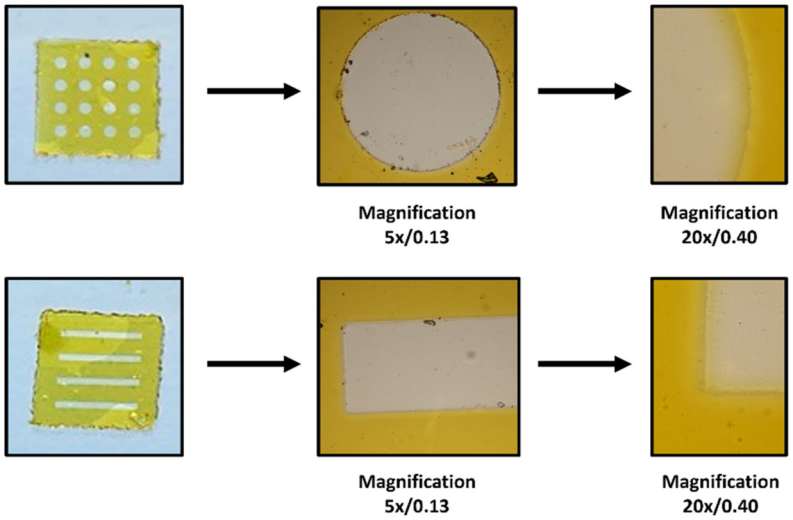

Fig. 6 Photochemical drawing on a cured film (10 mm × 10 mm) using 365 nm UV-light and a photomask (lined/dotted). Microscopic images with magnifications of 5×/0.13 and 20×/0.40 are presented for both films.

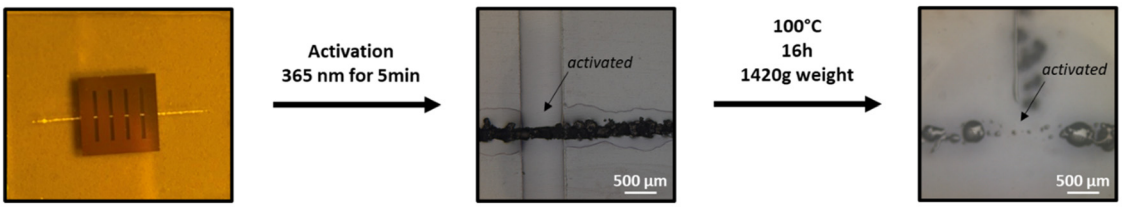

Fig. 7 Photopatterned-healing experiment of a cut in a cured film using a photomask. The healing of the cut is achieved by using 365 nm UV light to activate the **TMG-NOA**, followed by exposure to an elevated temperature of 100 °C and a 1420 g weight for 16 hours. The activated part is marked with an arrow.

The lined photomask was placed onto the cut and irradiated with 365 nm UV-light, to locally release the photolatent base **TMG-NOA**. Healing of the activated areas was achieved by applying pressure at 100 °C for 16 hours to induce the dynamic bond exchange reactions, as shown in Fig. 7. However, some non-activated parts of the cut also slowly started to heal based on mechanical deformation and physical relaxation of the network in the non-activated state or diffusion of the photogenerated base followed by thiol–thioester exchange reactions.

Conclusion

In this work, we have successfully synthesized and characterized novel TMG based photobases that enable spatially resolved activation of thiol–thioester exchange reactions in thiol–ene networks. By decoupling the network formation and dynamic exchange processes through selective wavelength control, curing could be achieved at 450 nm while the photobases were activated upon 365 nm light irradiation. The developed PLBs are accessible *via* a straightforward synthetic route that results in products with high purity and excellent yields. In addition, their very good solubility in thiol–ene networks enables homogeneous incorporation and ensures efficient, uniform activation. Among all synthesized photobases, **TMG-NOA** demonstrated outstanding performance in terms of spatiotemporal activation and catalytic efficiency. Furthermore, not only light but also temperature can be used to generate the active species on demand. The high catalytic efficiency allows dynamic bond exchange to proceed even at relatively low temperatures (40–70 °C), which is particularly advantageous for temperature-sensitive applications such as in the biomedical field. To further explore the versatility of the **TMG-NOA** containing networks, a series of experiments, including local imprinting, photopatterning, and locally induced healing, were conducted. The results of all these studies consistently support the concept of spatially controlled activation of the dynamic network upon exposure to 365 nm UV light.

Experimental

Materials

All chemicals were purchased from common suppliers and used as received. Pentaerythritol-tetrakis(3-mercaptopropio-

nate) (PETMP) (>90.0%) was obtained by TCI Deutschland GmbH. Succinic anhydride, 3-mercaptopropionic acid, 4-(dimethylamino) pyridine (≥99%), *p*-toluenesulfonic acid monohydrate (≥99%), allyl alcohol (≥98.5%), phenylglyoxylic acid (97%), triethylamine (≥99%), 1,1,3,3-tetramethylguanidine (99%) and bromothymol blue (95%) were purchased from Sigma-Aldrich. (Phenylphosphoryl)bis(mesitylmethanone) (BAPO) (99%), 1-(naphtalen-2-yl)ethanone, 2-(4-bromophenyl)-2-oxoacetic acid, 2-(4-ethylphenyl)-2-oxoacetic acid (95%) and 2-oxo-4-phenylbutanoic acid (97%) were received from BLDpharm and selenium dioxide was supplied by Fluka.

Synthesis of monomer

The synthesis of the primary thioester diacid (**1-TDA**) and the primary thioester diene (**TEDAE**) was carried out as described in literature with some minor deviations.[11,22] 1-TDA was purified by recrystallization in diethylether (68% yield). ^{1}H NMR (300 MHz, MeOD): δ 3.12 (t, 2H), 2.89 (t, 2H), 2.70–2.55 (m, 4H) ppm. TEDAE was filtrated through a silica pet and washed with toluene (90% yield). ^{1}H NMR (300 MHz, $CDCl_3$): δ 6.05–5.82 (m, 2H), 5.31 (dd, 4H), 4.63 (d, 4H), 3.18 (t, 2H), 2.92 (t, 2H), 2.76–2.63 (m, 4H) ppm.

Synthesis of precursor

The precursor 2-(naphthalen-2-yl)-2-oxoacetic acid was synthesizes by oxidation of 1-(naphthalene-2-yl)ethenone (8.0 mmol, 1.36 g,) using selenium dioxide (16 mmol, 1.78 g) and pyridine (4 mL), as described in literature (Scheme 1).[28] The resulting product was a yellow solid (7.4 mmol, 1.48 g, 92%). ^{1}H NMR (400 MHz, $CDCl_3$): δ 10.38–9.90 (bs, 1H), 9.16–9.00 (bs, 1H), 8.20–8.15 (d, 1H), 8.05–8.00 (d, 1H), 7.95–7.91 (d, 1H), 7.91–7.87 (d, 1H), 7.71–7.64 (t, 1H), 7.62–7.60 (t, 1H) ppm. ^{13}C NMR (400 MHz, $CDCl_3$): δ 184.2, 162.6, 136.7, 135.6, 132.4, 130.6, 130.2, 129.1, 128.0, 127.4, 124.7 ppm.

Synthesis of TMG-PLBs

The synthesis of 1,1,3,3-tetramethylguanidine phenylglyoxylate (**TMG-PGO**) was carried out as described in literature (Scheme 2).[22,25] ^{1}H NMR (400 MHz, $CDCl_3$): δ 9.06–8.80 (bs, 2H), 8.11–7.94 (d, 2H), 7.57–7.48 (m, 1H), 7.48–7.37 (m, 2H), 3.05–2.79 (bs, 12H) ppm.

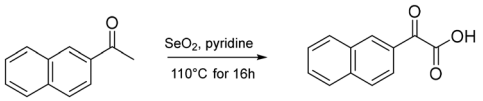

Scheme 1 Synthesis of the precursor 2-(naphthalen-2-yl)-2-oxoacetic acid.

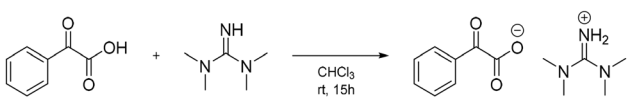

Scheme 2 Synthesis of 1,1,3,3-tetramethylguanidine phenylglyoxylate.

The corresponding derivatives containing 2-(4-bromophenyl)-2-oxoacetic acid, 2-(4-ethylphenyl)-2-oxoacetic acid, 2-oxo-4-phenylbutanoic acid (97%) and 2-(naphthalen-2-yl)-2-oxoacetic acid were synthesized using a modified approach based on the literature route of 1,1,3,3-tetramethylguanidine phenylglyoxylate. In a 50 mL two-necked round bottom flask equipped with a dropping funnel, 250 mg of the corresponding oxoacetic acid were dissolved in 10 ml chloroform and a solution of 1,1,3,3-tetramethylguanidine in 6 ml chloroform was added dropwise under vigorous stirring. The reaction was stirred for at least 15 h at room temperature. The work-up procedure varied depending on the oxoacetic acid used.

1,1,3,3-Tetramethylguanidine 2-(4-bromophenyl)-2-oxoacetate (TMG-BOA)

250 mg 2-(4-bromophenyl)-2-oxoacetic acid (1.1 mmol) and 0.137 ml 1,1,3,3-tetramethylguanidine (1.1 mmol, 126 mg) were used (Scheme 3). To precipitate the product, 25 mL of cold diethyl ether were added while cooling in an ice bath. The resulting off-white solid was filtered, washed repeatedly with diethyl ether and dried under vacuum (1.0 mmol, 353 mg, 94%). ^{1}H NMR (400 MHz, $CDCl_3$): δ 9.00–8.72 (bs, 2H), 7.93–7.84 (m, 2H), 7.58–7.50 (m, 2H), 2.96–2.88 (bs, 12H) ppm. ^{13}C NMR (400 MHz, $CDCl_3$): δ 195.0, 170.8, 162.4, 133.3, 131.7, 131.4, 128.0, 39.8 ppm.

1,1,3,3-Tetramethylguanidine 2-(4-ethylphenyl)-2-oxoacetate (TMG-EOA)

250 mg 2-(4-ethylphenyl)-2-oxoacetic acid (1.4 mmol) and 0.176 ml 1,1,3,3-tetramethylguanidine (1.4 mmol, 162 mg) were used (Scheme 4). To precipitate the product out of the reaction mixture 25 ml of cold diethyl ether were added while cooling in an ice bath. The resulting light-yellow solid was filtrated, washed repeatedly with diethyl ether and dried under vacuum (1.2 mmol, 350 g, 85%). ^{1}H NMR (400 MHz, $CDCl_3$): δ 9.07–8.78 (bs, 2H), 7.97–7.90 (d, 2H), 7.24–7.19 (d, 2H), 2.93–2.88 (bs, 12H), 2.69–2.61 (q, 2H), 1.23–1.17 (t, 3H) ppm. ^{13}C NMR (400 MHz, $CDCl_3$): δ 196.0, 171.8, 162.4, 149.9, 132.2, 130.0, 127.9, 39.8, 29.1, 15.4 ppm.

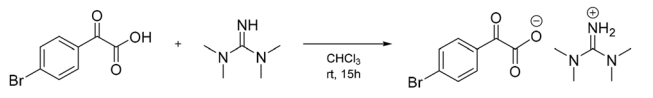

Scheme 3 Synthesis of 1,1,3,3-tetramethylguanidine 2-(4-bromophenyl)-2-oxoacetate.

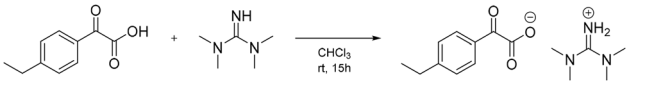

Scheme 4 Synthesis of 1,1,3,3-tetramethylguanidine 2-(4-ethylphenyl)-2-oxoacetate.

1,1,3,3-Tetramethylguanidine 4-phenylbutoxy acetate (TMG-PBA)

250 mg 2-oxo-4-phenylbutanoic acid (1.4 mmol) and 0.176 ml 1,1,3,3-tetramethylguanidine (1.4 mmol, 162 mg) were used (Scheme 5). For the purification 25 mL of cold diethyl ether were added. Since no precipitation occurred, the solvent was removed under vacuum. The resulting product was an orange oil (1.1 mmol, 330 mg, 80%). ^{1}H NMR (400 MHz, $CDCl_3$): δ 9.43–8.14 (bs, 1H), 7.25–7.10 (m, 5H), 3.11–3.10 (t, 2H), 2.96–2.92 (bs, 12H), 2.92–2.87 (t, 2H) ppm. ^{13}C NMR (400 MHz, $CDCl_3$): δ 204.8, 169.3, 162.4, 141.7, 128.5, 128.4, 125.8, 41.2, 39.8, 29.5 ppm.

1,1,3,3-Tetramethylguanidine 2-(naphthalen-2-yl)-2-oxoacetate (TMG-NOA)

250 mg 2-(naphthalen-2-yl)-2-oxoacetic acid (1.2 mmol) and 0.157 ml 1,1,3,3-tetramethylguanidine (1.2 mmol, 144 mg) were used. For the purification of the product, 25 mL of cold diethyl ether were added (Scheme 6). Since no precipitation occurred, the solvent was removed under vacuum. The resulting product was a viscous orange oil (1.1 mmol, 342 mg, 87%). ^{1}H NMR (400 MHz, $CDCl_3$): δ 8.65–8.59 (bs, 1H), 8.17–8.04 (dd, 1H), 7.96–7.90 (d, 1H), 7.90–7.74 (m, 2H), 7.57–7.49 (m, 1H), 7.49–7.39 (m, 1H), 2.90–2.87 (bs, 12H) ppm. ^{13}C NMR (400 MHz, $CDCl_3$): δ 196.3, 171.7, 162.4, 135.8, 132.7, 132.6, 131.7, 129.8, 128.3, 128.2, 127.8, 126.5, 124.7, 39.8 ppm.

Nuclear magnetic resonance spectroscopy

^{1}H and ^{13}C NMR spectra were recorded on a Jeol JNM-ECZL 400 MHz spectrometer or Bruker Avance 300 MHz in either MeOD or $CDCl_3$. The chemical shifts were measured in parts per million [ppm]. The reference used was TMS (0.00 ppm for ^{1}H and ^{13}C).

UV-Vis spectrometry

UV-Vis absorption spectra were obtained in acetonitrile using a Shimadzu UV-1800 spectrophotometer, covering a wavelength range of 200–800 nm. For the measurements a quartz cuvette with an optical path length of 10.00 mm was used.

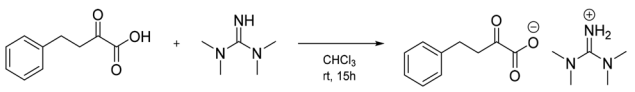

Scheme 5 Synthesis of 1,1,3,3-tetramethylguanidine 4-phenylbutoxy acetate.

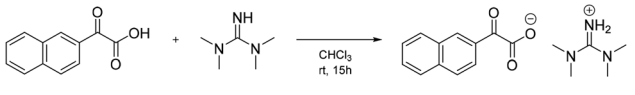

Scheme 6 Synthesis of 1,1,3,3-tetramethylguanidine 2-(naphthalen-2-yl)-2-oxoacetate.

pH measurements

The pH measurements in methanol were carried out on a SevenDirect SD20 from Mettler Toledo with an InLab Science Pro-ISM electrode. For the measurements, the corresponding TMG-PLBs (1.2 mmol) were dissolved in 20 mL methanol (0.06 M). The pH was measured under moderate stirring (400 rpm). The solution was first irradiated with 450 nm LED light (LED Control 5S spot, 100% lamp intensity) to ensure the inactivity of the photolatent base. To monitor the release of the photolatent base, the solutions were irradiated with 365 nm LED light (LED Control 5S spot instrument from Opsytec Dr Gröbl (Germany), 100% lamp intensity) under moderate stirring (400 rpm). The light guide was place at a distance of 4 cm from the surface of the liquid. The irradiation was interrupted for the pH measurements.

Resin preparation

BAPO (1 mol% relative to the thiol functions, 8.19×10^{-2} mmol, 34 mg) was dissolved in 1TE-diene (2.05 mmol, 586 mg) by sonication for 80 minutes. Then, the corresponding TMG-PLB (3 mol% relative to the thiol functions, 2.46×10^{-1} mmol) and PETMP (2.05 mmol, 1.00 g) were added and dissolved by sonication or stirring on a metal heating block at 30 °C (Table 1).

Specimen preparation

Two glass plates were coated three times with the release agent Chemlease® 2720 from ChemTrend. The thiol–ene resin containing the corresponding TMG-PLB was loaded between the two glass slides spaced 0.50 mm apart, and irradiated to complete conversion (450 nm, LED Control 5S spot, 100% lamp intensity, distance sample to light guide 8 cm, 10 min per side). For DSC and TGA samples, the film was activated with 365 nm for 1 min per side (LED Control 5S spot instrument from Opsytec Dr Gröbl (Germany), 100% lamp intensity, distance sample to light guide 5 cm). For Zeta potential samples the film was activated with 365 nm for 10 min on one side (LED Control 5S spot instrument from Opsytec Dr Gröbl (Germany), 100% lamp intensity, distance sample to light guide 10 cm). For stress relaxation samples circular specimens (10 mm × 0.5 mm) were punched out of the film. The light-mediated activation of the specimen was carried out by irradiating the samples with 365 nm for 1 min per side (LED Control 5S spot instrument from Opsytec Dr Gröbl (Germany),

Table 1 Weighted TMG-PLBs with corresponding dissolving time through sonication or heating block

TMG-PLB	Mass [mg]	Sonication time [min]	Heating block [min]
TMG-PGO	65.2	15	
TMG-BOA	72.0		20
TMG-EOA	84.5	15	
TMG-PBA	72.0	10	
TMG-NOA	77.4	10	

100% lamp intensity, distance sample to light guide 5 cm). The thermal activation was performed by incubating the sample in the oven at 125 °C for 30 minutes.

Rheological investigations

Non-activated and activated specimens were measured using an Anton Paar Physica MCR-501 rheometer in parallel plate configuration. The measurements were carried out at temperatures between 40 °C and 80 °C, and each sample was equilibrated to the measurement temperature with a constant normal force of 5 N for 10 min. Afterwards a 3% step strain was applied and the relaxation modulus was monitored over time.

FTIR spectroscopy

The curing kinetics were carried out using a Bruker Avance P infrared spectrometer with ATR accessory. 16 scans were measured at a resolution of 4 cm^{-1} and a range from 4000 to 800 cm^{-1}. One drop of resin was spread between two calcium fluoride discs and measured using the ATR accessory. The discs were illuminated with 450 nm LED light (LED Control 5S spot instrument from Opsytec Dr Gröbl, 20% intensity) at a distance of 20 cm.

Differential scanning calorimetry

DSC measurements were performed on a Differential Scanning Calorimeter DSC 8500 with Hyper DSC from PerkinElmer. The measurements were conducted with about 10 mg of sample and a temperature program consisting of two heating rates (heating rate 1 : 10 K min^{-1}, heating rate 2 : 40 K min^{-1}) under nitrogen atmosphere. The corresponding glass transition temperatures were determined from the first heating cycle as the midpoint in heat capacity.

Thermogravimetric analysis

TGA measurements were performed on a PerkinElmer TGA 8000 using about 2.0 mg of sample. The measurements were carried out under nitrogen flow (20.0 ml min^{-1}) in a temperature range of 30 °C to 400 °C with a heating rate of 10 °C min^{-1}.

Zeta-potential measurements

The zeta potential ζ of the sample surfaces was determined by the streaming potential method, using the adjustable gap cell (AGC) connected with the SurPASS 2 an electrokinetic analyzer (Anton Paar GmbH, Graz, Austria). For the AGC two samples with 20 mm × 10 mm are fixed on sample holders using double-sided adhesive tape. The distance between the samples' surfaces is then adjusted continuously. For AGC, the complete sample surface is used for measurement (100% of total sample area). In this cell, the electrolyte is pressed through a flow channel created by the two parallel clamped sample surfaces at a distance of 100 μm. Measurements were made at 24 ± 2 °C and for a maximum pressure difference of 600 mbar with flow in the two directions. The measurements were performed with a KCl electrolyte solution (10^{-3} M, 600 mL). Experiments startet at pH 5.5 ± 0.2 pH was adjusted by adding HCl (0.05 M). Solutions of KCl (1 mM, 5 mM or 10 mM) served as the electrolyte for the measurements of the samples. The solutions were prepared using high-purity water (Milli-Q, Millipore).

Imprinting

The resin was poured into a silicon mold (25 × 25 × 2 mm) and covered with a release agent coated glass plate. The curing of the films was achieved using an 450 nm LED light (LED Control 5S spot instrument from Opsytec Dr Gröbl, 100% intensity) at a distance of 8 cm over 10 minutes. One part of the film was covered completely with aluminium foil and the other one was irradiated with 365 nm at a distance of 5 cm (LED Control 5S spot instrument from Opsytec Dr Gröbl, 100% intensity) for 2 minutes to activate the photolatent base. The films were placed in a self-manufactured Teflon press, where the pressure can be adjusted with screws. As imprinting objects, two 1-euro coins (backside of the coins: (1) the Vitruvian man (2) Beatrix, queen of the Netherlands) were placed on the films. The Teflon press was then placed in an oven for 15 minutes at 70 °C, after cooling the pressure was released to reveal the imprints on the activated side. Microscopic images were recorded using a wide-angle feature.

Spatial activation using a photomask

6 mg of bromothymol blue were dissolved in the prepared resin and loaded between two release agent coated glass slides with a 0.3 mm spacer. The resin was irradiated to complete conversion with 450 nm UV-light (10 min per side, 8 cm distance). Then, the photomasks (lined and dotted) were placed on the film and irradiated with 365 nm UV-light (5 min, 5 cm distance). Microscopic images were recorded with a magnification of 5×/0.13 and 20×/0.40.

Healing

The resin was loaded between two release agent coated glass slides with a 0.5 mm spacer and irradiated to complete conversion with 450 nm UV-light (10 min per side, 8 cm distance). One small cut was made using a scalpel and the lined photomask was placed onto it and irradiated with 365 nm UV-light (5 min, 5 cm distance). Afterwards, the photomask was removed and a microscopic image was recorded. A glass plate was then placed on the film, and the sample was heated in the oven at 100 °C for 16 hours with a 1420 g weight applied on top. After cooling, the self-healed area was revealed. Microscopic images were recorded with a magnification of 5×/0.13.

Conflicts of interest

There are no conflicts to declare.

Data availability

The data supporting this article have been included as part of the supplementary information (SI). Supplementary information is available. See DOI: https://doi.org/10.1039/d5py00779h.

Acknowledgements

"Funded by the European Union. Views and opinions expressed are however those of the author(s) only and do not necessarily reflect those of the European Union or the granting authority European Union's Horizon Europe research and innovation programme. Neither the European Union nor the granting authority can be held responsible for them. The DECIPHER project has received funding under the Horizon Europe research and innovation programme (the grant agreement no. 101137242)".

The research work was performed at the Polymer Competence Center Leoben GmbH (PCCL, Austria) within the framework of the COMET-program of the Federal Ministry for Transport, Innovation and Technology and the Federal Ministry of Science, Research and Economy with contributions by academic and commercial partners. The PCCL is funded by the Austrian Government and the State Governments of Styria, Lower Austria and Upper Austria.

References

1 C. J. Kloxin, T. F. Scott, B. J. Adzima and C. N. Bowman, Covalent Adaptable Networks (CANs): A Unique Paradigm in Crosslinked Polymers, *Macromolecules*, 2010, **43**(6), 2643–2653, DOI: 10.1021/ma902596s.

2 G. Zhang, Q. Zhao, L. Yang, W. Zou, X. Xi and T. Xie, Exploring Dynamic Equilibrium of Diels-Alder Reaction for Solid State Plasticity in Remoldable Shape Memory Polymer Network, *ACS Macro Lett.*, 2016, **5**(7), 805–808, DOI: 10.1021/acsmacrolett.6b00357, published Online: Jun. 21, 2016.

3 A. Gandini, The furan/maleimide Diels–Alder reaction: A versatile click–unclick tool in macromolecular synthesis, *Prog. Polym. Sci.*, 2013, **38**(1), 1–29, DOI: 10.1016/j.progpolymsci.2012.04.002.

4 B. T. Worrell, S. Mavila, C. Wang, T. M. Kontour, C.-H. Lim, M. K. McBride, C. B. Musgrave, R. Shoemaker and C. N. Bowman, A user's guide to the thiol-thioester exchange in organic media: scope, limitations, and applications in material science, *Polym. Chem.*, 2018, **9**(36), 4523–4534, DOI: 10.1039/C8PY01031E.

5 B. T. Worrell, M. K. McBride, G. B. Lyon, L. M. Cox, C. Wang, S. Mavila, C.-H. Lim, H. M. Coley, C. B. Musgrave, Y. Ding and C. N. Bowman, Bistable and photoswitchable states of matter, *Nat. Commun.*, 2018, **9**(1), 2804, DOI: 10.1038/s41467-018-05300-7, published Online: Jul. 18, 2018.

6 C. N. Bowman and C. J. Kloxin, Toward an enhanced understanding and implementation of photopolymerization reactions, *AIChE J.*, 2008, **54**(11), 2775–2795, DOI: 10.1002/aic.11678.

7 C. R. Morgan, F. Magnotta and A. D. Ketley, Thiol/ene photocurable polymers, *J. Polym. Sci., Polym. Chem. Ed.*, 1977, **15**(3), 627–645, DOI: 10.1002/pol.1977.170150311.

8 M. A. Lucherelli, A. Duval and L. Avérous, Biobased vitrimers: Towards sustainable and adaptable performing polymer materials, *Prog. Polym. Sci.*, 2022, **127**, 101515, DOI: 10.1016/j.progpolymsci.2022.101515.

9 T. Vidil and A. Llevot, Fully Biobased Vitrimers: Future Direction toward Sustainable Cross-Linked Polymers, *Macromol. Chem. Phys.*, 2022, **223**(13), 2100494, DOI: 10.1002/macp.202100494.

10 B. Sölle, D. Reisinger, S. Heupl, A. Jelinek, S. Schlögl and E. Rossegger, Reshapable bio-based thiol-ene vitrimers for nanoimprint lithography: Advanced covalent adaptability for tunable surface properties, *React. Funct. Polym.*, 2024, **202**, 105972, DOI: 10.1016/j.reactfunctpolym.2024.105972.

11 N. J. Bongiardina, K. F. Long, M. Podgórski and C. N. Bowman, Substituted Thiols in Dynamic Thiol–Thioester Reactions, *Macromolecules*, 2021, **54**(18), 8341–8351, DOI: 10.1021/acs.macromol.1c00649.

12 M. Podgórski, N. Spurgin, S. Mavila and C. N. Bowman, Mixed mechanisms of bond exchange in covalent adaptable networks: monitoring the contribution of reversible exchange and reversible addition in thiol–succinic anhydride dynamic networks, *Polym. Chem.*, 2020, **11**(33), 5365–5376, DOI: 10.1039/D0PY00091D.

13 D. Reisinger, K. Dietliker, M. Sangermano and S. Schlögl, Streamlined concept towards spatially resolved photoactivation of dynamic transesterification in vitrimeric polymers by applying thermally stable photolatent bases, *Polym. Chem.*, 2022, **13**(9), 1169–1176, DOI: 10.1039/D1PY01722E.

14 O. Konuray, S. Moradi, A. Roig, X. Fernández-Francos and X. Ramis, Thiol–Ene Networks with Tunable Dynamicity for Covalent Adaptation, *ACS Appl. Polym. Mater.*, 2023, **5**(3), 1651–1656, DOI: 10.1021/acsapm.2c02136.

15 B. Sölle, M. Schmallegger, S. Schlögl and E. Rossegger, Wavelength-Dependent Dynamic Behavior in Thiol-Ene Networks Based on Disulfide Exchange, *J. Am. Chem. Soc.*, 2024, **146**(49), 34152–34157, DOI: 10.1021/jacs.4c13735, published Online: Dec. 1, 2024.

16 V. S. Khire, Y. Yi, N. A. Clark and C. N. Bowman, Formation and Surface Modification of Nanopatterned Thiol–ene Substrates using Step and Flash Imprint Lithography, *Adv. Mater.*, 2008, **20**(17), 3308–3313, DOI: 10.1002/adma.200800672.

17 L. Brigo, T. Carofiglio, C. Fregonese, F. Meneguzzi, G. Mistura, M. Natali and U. Tonellato, An optical sensor for pH supported onto tentagel resin beads, *Sens. Actuators, B*, 2008, **130**(1), 477–482, DOI: 10.1016/j.snb.2007.09.020.

18 Z. T. Cygan, J. T. Cabral, K. L. Beers and E. J. Amis, Microfluidic platform for the generation of organic-phase microreactors, *Langmuir*, 2005, **21**(8), 3629–3634, DOI: 10.1021/la0471137.

19 J. Ahn, Y. Lee, J. Kim, S. Yoon, Y.-C. Jeong and K. Y. Cho, Thiol-ene UV-curable sponge electrolyte for low-voltage color changing wearable tactile device, *Polymer*, 2022, **250**, 124898, DOI: 10.1016/j.polymer.2022.124898.

20 P. M. Kharkar, M. S. Rehmann, K. M. Skeens, E. Maverakis and A. M. Kloxin, Thiol-ene click hydrogels for therapeutic delivery, *ACS Biomater. Sci. Eng.*, 2016, **2**(2), 165–179, DOI: 10.1021/acsbiomaterials.5b00420, published Online: Jan. 11, 2016.

21 X. Li and Y. Xiong, Application of "Click" Chemistry in Biomedical Hydrogels, *ACS Omega*, 2022, **7**(42), 36918–36928, DOI: 10.1021/acsomega.2c03931, published Online: Oct. 12, 2022.

22 D. Reisinger, A. Hellmayr, M. Paris, M. Haas, T. Griesser and S. Schlögl, Spatially resolved photoactivation of dynamic exchange reactions in 3D-printed thiol–ene vitrimers, *Polym. Chem.*, 2023, **14**(26), 3082–3090, DOI: 10.1039/D3PY00377A.

23 D. Reisinger, M. U. Kriehuber, M. Bender, D. Bautista-Anguís, B. Rieger and S. Schlögl, Thermally Latent Bases in Dynamic Covalent Polymer Networks and their Emerging Applications, *Adv. Biomater.*, 2023, **35**(24), e2300830, DOI: 10.1002/adma.202300830, published Online: Apr. 27, 2023.

24 D. Reisinger, A. Sietmann, A. Das, S. Plutzar, R. Korotkov, E. Rossegger, M. Walluch, S. Holler-Stangl, T. S. Hofer, F. Dielmann, F. Glorius and S. Schlögl, Light-Driven, Reversible Spatiotemporal Control of Dynamic Covalent Polymers, *Adv. Biomater.*, 2024, **36**(47), e2411307, DOI: 10.1002/adma.202411307, published Online: Oct. 6, 2024.

25 H. Salmi, X. Allonas, C. Ley, A. Defoin and A. Ak, Quaternary ammonium salts of phenylglyoxylic acid as photobase generators for thiol-promoted epoxide photopolymerization, *Polym. Chem.*, 2014, **5**(22), 6577–6583, DOI: 10.1039/C4PY00927D.

26 M. Paul, K. Peckelsen, T. Thomulka, J. Neudörfl, J. Martens, G. Berden, J. Oomens, A. Berkessel, A. J. H. M. Meijer and M. Schäfer, Hydrogen tunneling avoided: enol-formation from a charge-tagged phenyl pyruvic acid derivative evidenced by tandem-MS, IR ion spectroscopy and theory, *Phys. Chem. Chem. Phys.*, 2019, **21**(30), 16591–16600, DOI: 10.1039/c9cp02316j, published Online: Jul. 18, 2019.

27 T. Shimada and T. Hasegawa, Determination of equilibrium structures of bromothymol blue revealed by using quantum chemistry with an aid of multivariate analysis of electronic absorption spectra, *Spectrochim. Acta A Mol. Biomol. Spectrosc.*, 2017, **185**, 104–110, DOI: 10.1016/j.saa.2017.05.040, published Online: May. 19, 2017.

28 Z. Zheng, Y. Wu, X. Lu, F.-L. Zhang, M.-F. Qi, E. Sun and B. Sun, Visible-light-mediated metal-free decarboxylative acylation of electron-deficient quinolines using α-ketoacids under ambient air, *Tetrahedron*, 2022, **112**, 132749, DOI: 10.1016/j.tet.2022.132749.